Influencing Particle Size and Stability of Ionic Dendrimer−Dye Assemblies

Immanuel Willerich,[†] Yi Li,[‡] and Franziska Gröhn*,[†]

Department of Chemistry and Pharmacy and Interdisciplinary Center for Molecular Materials, Friedrich-Alexander-University Erlangen-Nürnberg, Egerlandstrasse 3, 91058 Erlangen, Germany and Max Planck Institute for Polymer Research, Ackermannweg 10, D-55128 Mainz, Germany

Received: August 5, 2010; Revised Manuscript Received: October 4, 2010

This article focuses on the physical chemical aspects of the formation of supramolecular nanoparticles with defined size and varying shape through electrostatic self-assembly of macroions and multivalent aromatic counterions. For cationic poly(amidoamine) dendrimers and different di- and trivalent sulfonate groups carrying azo dyes, the onset of interdendrimer connection and assembly size (hydrodynamic radius 20 nm $< R_h <$ 150 nm) depend on counterion/macroion loading ratio. Centrifugation and dialysis experiments show assemblies coexisting with individual dye-loaded dendrimers with lower dye/dendrimer ratio at small loading ratio, while around charge stoichiometry only assemblies are present. Zeta-potential measurements reveal a positive charge for samples with excess dendrimer. For excess dye, overloading to negatively charged assemblies is possible for some dyes, which is consistent with concentration-dependent stability revealing a second mode of more loosely bound dye ions. Kinetic versus thermodynamic effects are discussed based on varying the preparation route. The interaction enthalpy is an important factor in determining assembly size. Solution structures are characterized by static and dynamic light scattering, while atomic force microscopy showed that assemblies can also be deposited on surfaces.

Introduction

The creation of supramolecular nanostructures from small building blocks is of high versatility, as their properties can be easily tailored by variations in the compound structure.[1−4] Many supramolecular self-assembled systems are well established and can serve for a wide range of applications for example in optoelectronics, sensors, or drug delivery systems, especially due to their responsiveness to various external triggers.[5−14] Self-assembly can be based on different interactions like hydrogen bonding,[15−18] metal coordination,[15,19−23] amphiphilicity,[24−26] ionic interactions,[27−34] or rely on more specific binding motifs.[35−37] Assembly formation of π-conjugated molecules is currently an emerging field, as those molecules have interesting properties and capabilities like fluorescence and charge transfer which can be tuned by changing the aggregation state.[38−50]

Recently, we have shown the concept of electrostatic self-assembly of polyelectrolytes and multivalent structured organic dye counterions to represent a facile pathway to supramolecular particles in solution, the dimensions of which lie in the size range of about 10-fold the size of the building blocks.[51−61] In this approach, electrostatic interactions in combination with mutual $\pi-\pi$-interaction of the dye counterions or geometric factors are the driving forces leading to the formation of assemblies with a variety of shapes and with narrow size distribution.[62] The advantage and versatility of the concept lie in its simplicity as the nanostructures in solution can be created by simply mixing building blocks which are readily available and no specific motifs are required. This is different from known electrostatically self-assembled systems like dye−surfactant or polyelectrolyte−surfactant systems representing periodic materials in the solid state,[9,27,28,30,63−65] layer-by-layer thin film systems, which require a multistep fabrication procedure,[66−70] or aggregates from oppositely charged polyelectrolytes and polyelectrolytes with nonstructural counterions, which form in solution but where structural control is limited,[29,71−74] unless semiflexible building blocks are introduced as was described recently.[31,75,76] Also from a more theoretical point of view, the building block structure on the mesoscale has been identified as a key feature for the formation of complex assemblies.[77,78]

In two previous studies, we investigated self-assembly in a model system of fourth generation poly(amidoamine) dendrimer (G4 PAMAM) as cationic macroion and a set of anionic aromatic azo dyes (Scheme 1).[52,55] We showed with small-angle neutron scattering (SANS) that assemblies with different shapes like cylinders, spheres, or core−shell structure in the size range of 100 nm comprising multiple dendrimers can be formed depending on the dye structure. Charge stoichiometry turned out to be a crucial parameter as was shown by UV−vis spectroscopy and isothermal titration calorimetry (ITC). Further, it was proven that electrostatic interaction and $\pi-\pi$ interaction are the driving forces for assembly formation, the latter accounting approximately for 60% of the total interaction enthalpy.

To be able to tailor the properties of dendrimer−dye assemblies, further fundamental understanding of their aggregation behavior is required. The main objectives of this study are to further understand the conditions of assembly stability, to investigate the extent to which assemblies get interconnected by the dye molecules on a quantitative level, and to correlate particle sizes with association enthalpies and equilibrium constants of the assembly formation. In addition, elucidating the influence of preparation method is a key point. In the following, first, a light scattering study will be presented together with complementary atomic force microscopy (AFM) images, in which the assemblies of G4 PAMAM dendrimer and the azo dyes Ar18, Ar26, Ar27, and Ar44 are compared (Scheme 1).

* Corresponding author. Fax: 49-9131-85 28307. E-mail: Franziska.Groehn@chemie.uni-erlangen.de.
[†] Friedrich-Alexander-University Erlangen-Nürnberg.
[‡] Max-Planck-Institute for Polymer Research, Mainz.

10.1021/jp107358q
Published on Web 11/05/2010

SCHEME 1: Building Blocks for Electrostatic Self-Assembly Used in This Study and Sketch of the Assembly Formation: Dendrimer and Dye Building Blocks Associate into Larger Structures Due to Ionic and $\pi-\pi$ Interaction[a]

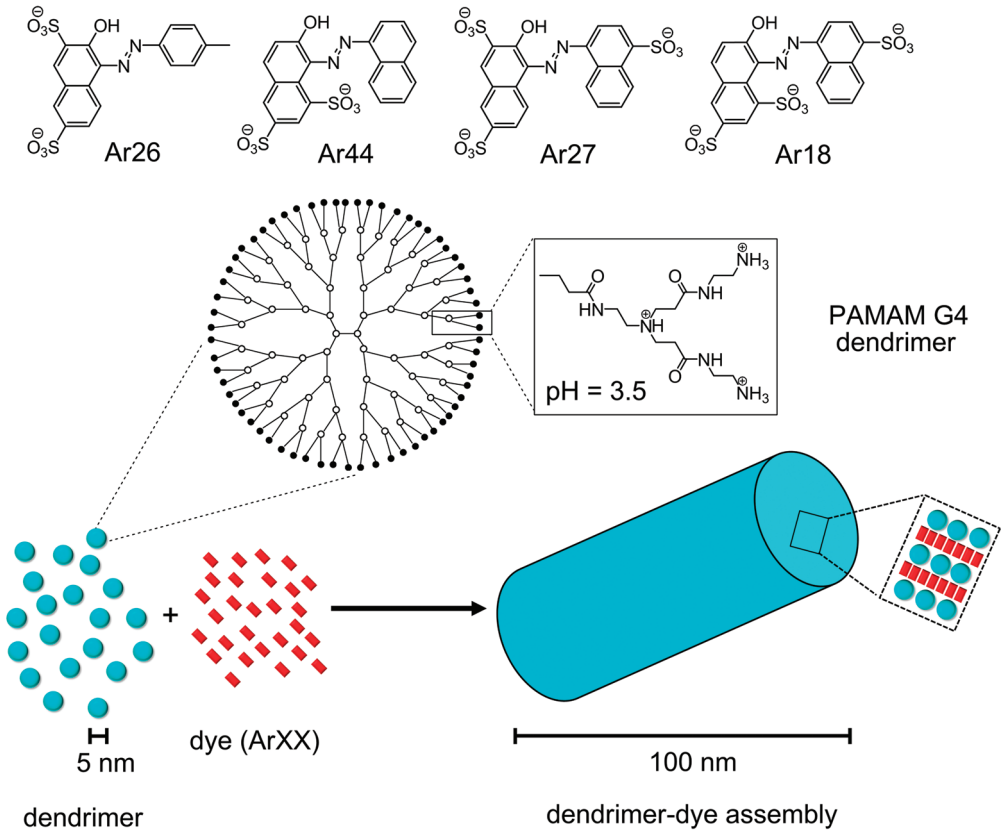

[a] The cylindrical shape represents an example, as assembly shape depends on the dye applied.

Zeta-potential measurements are employed to understand the stability of the colloidal assemblies. The equilibrium between single and interconnected dendrimers incorporated in larger assemblies was investigated using centrifugation and dialysis experiments. Finally, the influence of kinetics is probed by comparing different preparation methods and evaluating their effect on the assembly characteristics. Based on these results, a general model is proposed on how characteristics of the building blocks correlate with the assembly features.

As reported previously, the loading ratio l is defined as the ratio of the molar concentration of dye sulfonate groups to the molar concentration of dendrimer primary amine groups:

$$l = \frac{c(\mathrm{SO_3H, counterion})}{c(\mathrm{NH_2, dendrimer})} \quad (1)$$

After mixing the building blocks at pH = 10.5, we adjusted the pH to pH = 3.5, protonating all dendrimer amino groups.[55] Thus, charge stoichiometry corresponds to $l \approx 2$ for all samples as there is also about one tertiary amino group for each primary amino group.

Experimental Section

Chemicals. Generation 4 poly(amidoamine) dendrimer was obtained from Dendritech, Midland, MI. Radius and size distribution given by the supplier were confirmed by DLS and HPLC. Acid Red dyes were obtained from Acros, Geel, Belgium (Ar26, Ar44, Ar27, Ar18). They were recrystallized five times from ethanol and dried in vacuum. Purity was checked by ^{1}H NMR, elemental analysis, and extinction coefficient. No detectable organic impurities remain by this procedure. Concentrations were corrected for the remaining amount of inorganic salts (which do not influence our measurements as they do not influence aggregation behavior substantially).

Sample Preparation. Stock solutions were prepared in Milli-Q ultrapure water (>18.2 MΩ/cm) at the desired pH (either pH = 3.5 or pH = 10.5, see below). pH values were adjusted by adding the calculated amount of NaOH or HCl standard solutions. All pH values were counterchecked by a freshly calibrated pH electrode. The standard dendrimer concentration in this study was $c = 0.04$ g L^{-1}.

Preparation at low pH, method I (mI): an aqueous stock solution of the dye at pH = 3.5 was diluted with Milli-Q ultrapure water adjusted to pH = 3.5. The G4 PAMAM dendrimer stock solution of the same pH was added and the sample was shaken immediately for 30 s for fast mixing. This is identical with the previously reported procedure.

Preparation at high pH, method II (mII): an aqueous solution of the dye at pH = 10.5 was diluted with Milli-Q ultrapure water adjusted to pH = 10.5. Dendrimer stock solution at the same pH was added. After mixing, the appropriate amount of HCl was added at once under turbulent mixing to adjust the sample pH to 3.5 inducing assembly formation.

Light Scattering. Measurements were carried out using an ALV 5000 correlator with 320 channels (ALV Langen, Germany) and a HeNe laser with a wavelength of $\lambda = 632.8$ nm with 22 mW output power. A range of scattering angles of $30° \le \theta \le 150°$ was covered. Measurement and data analysis were as established. The time autocorrelation function of the scattered intensity was measured and converted into the scattered electric field autocorrelation function via Siegert relation. The electric

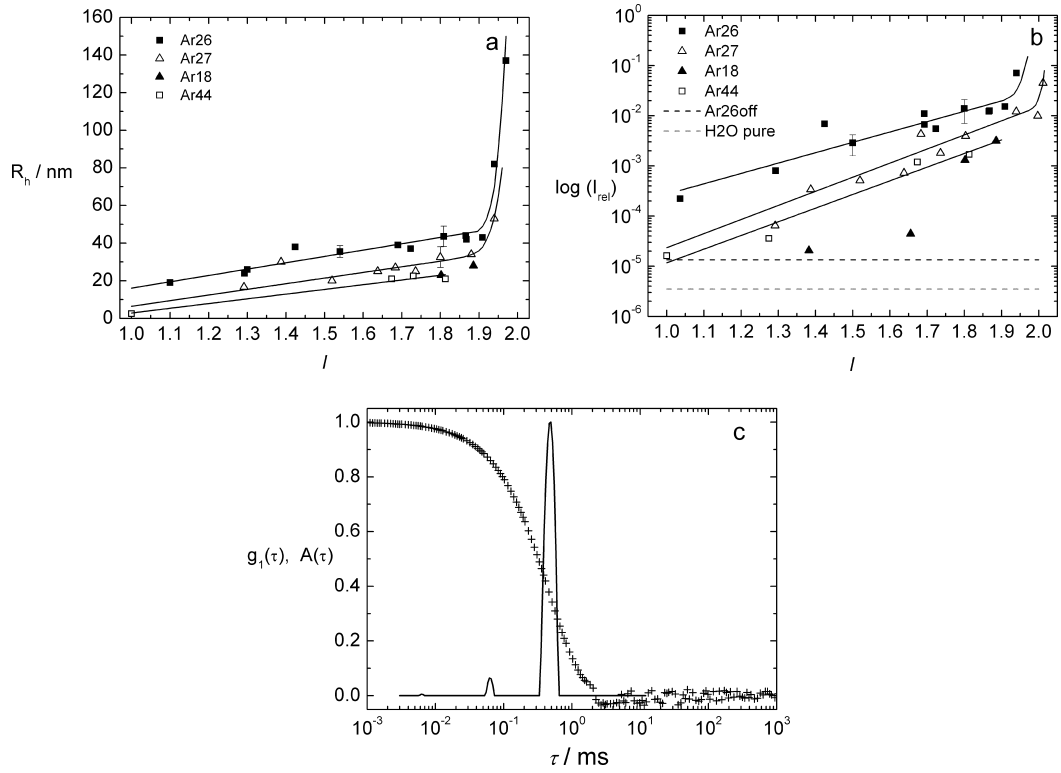

Figure 1. (a) Hydrodynamic radii R_h and (b) relative scattering intensities I_{rel} for dendrimer−dye assemblies with Ar26, Ar27, Ar18, and Ar44; c(G4) = 0.04 g L^{-1}, preparation according to method II; all values in (a) and (b) result from extrapolation to zero scattering angle, and lines are to guide the eye. (c) Typical correlation function and distribution of relaxation times for an Ar26/G4 sample with $l = 1.8$ at a scattering angle of $\theta = 90°$.[82]

field autocorrelation functions were analyzed by inverse Laplace transformation using the program CONTIN by S. Provencher[79] or by stretched exponential fits. The apparent diffusion coefficient was calculated from the inverse relaxation time and extrapolated to zero scattering vector square. Hydrodynamic radii were obtained via Stokes−Einstein relation from diffusion coefficients.

Zeta Potential. Measurements were conducted on a PSS Nicomp 380 ZLS with 0.9 cm electrode distance at a voltage of 10 V/cm. Usually four runs with each 90 s were used. Only measurements where a stable value was reached were included. The Smoluchowski formula was used to calculate electrophoretic mobility and ζ-potential as there is about 1 mmol low molecular mass salt in the solution from pH adjustment.

UV−Vis Spectroscopy. Absorption spectra were recorded on a Lambda 25 spectrometer from Perkin-Elmer using quartz cuvettes with 1 cm path length.

Centrifugation. Centrifugation was carried out on a Sigma 3-30K centrifuge at 25 000 rpm/minimal radius 5 cm in 2.2 mL tubes.

Dialysis. Dialysis was carried out in Float-a-lyzer dialysis tubes from Sigma-Aldrich with a molecular weight cutoff of 100 kDa for 2 weeks with Milli-Q water adjusted to pH = 3.5.

AFM. AFM images were recorded on a NanoSurf Easy Scan instrument (Boston, MA) and on a MultiMode Nanoscope IIIa Atomic Force Microscope (Veeco Instruments, CA) in tapping mode. For images in Figure 2 and 3, a silicon cantilever (OMCLAC 160 TS-W, Olympus, Japan) with 42 N m^{-1} spring constant and nominal tip radius <10 nm was used. Typical imaging parameters were as follows: working frequencies of 300−400 kHz, a working oscillation amplitude of 1.0−1.5 V, a scan rate of 1 Hz; and an image resolution of 512 × 512 pixels. The raw topography data were processed by flattening to remove the background slope. Typically, a 3−10 μL sample aliquot was dropped onto freshly cleaved mica, rinsed with 5 mL of Milli-Q water, and then blow dried with compressed air immediately. The program Nanoscope 5.31r1 (Veeco, CA) was used for statistical analysis.

NMR Spectroscopy. A Bruker Avance 300 at 300 MHz with 256 scans was used. D_2O served as solvent. Defined amounts of NaOD were added to dissolve assemblies for NMR.

Results and Discussion

A. Size and Shape of Dendrimer−Dye Assemblies Analyzed by Light Scattering and Atomic Force Microscopy. To compare assembly sizes of complexes consisting of fourth generation PAMAM dendrimer and the azo dyes given in Scheme 1 quantitatively, a large set of samples with moderate dendrimer amino group excess ($1 < l < 2$) was prepared according to preparation method II and examined by static and dynamic light scattering (SLS and DLS). Hydrodynamic radii and scattering intensities of assemblies of Ar18, Ar26, Ar27, and Ar44 with excess of cationic G4 dendrimer as function of charge ratio and the correlation function and relaxation time distribution of a typical Ar26/G4 sample are depicted in Figure 1. For lower loading ratios $l < 1$ usually no larger aggregates were found, whereas samples with loading ratios higher than $l = 2$ are not time stable.

For Ar26, hydrodynamic radii increase from about $R_h = 20$ nm for $l \approx 1$ to about $R_h = 43$ nm for $l = 1.8$. Close to charge stoichiometry at $l \approx 1.95$, sizes increase to $R_h > 100$ nm and at this concentration precipitation occurs after a few days to weeks. To study the reproducibility of the sizes, a set of 16 samples was investigated for $l = 1.8$. The standard deviation of radii from different samples is about 14% ($R_h = 43 \pm 6$ nm, $R_g = 52 \pm 8$ nm, $R_g/R_h = 1.19 \pm 0.067$). Size distributions are very narrow as evident from Figure 1c ($\sigma = 0.15 \pm 0.05$).[80] For $l = 1.5$, results are similar ($R_h = 36 \pm 3$ nm, $\sigma = 0.21 \pm 0.04$, R_g

= 41 ± 3.5 nm, R_g/R_h = 1.16 ± 0.12, average over four samples). Radii of gyration increase from R_g = 30 nm to R_g = 60 nm for the same loading ratios, and R_g/R_h values range between 1.1 and 1.3, indicating a nonspherical shape. The dependency of the scattering intensity on the loading ratio is given in Figure 1b. It can be exploited to determine the point where only individual dendrimers loaded with dye are present:[81] in the "off" state at pH = 10.5 all dendrimer amino groups are deprotonated so that the dendrimer is uncharged. Thus, no electrostatic binding process and therefore no assembly formation takes place and only individual dendrimer molecules and unbound dye ions are present.[52] When the scattering intensity of a sample in "on" state (pH = 3.5) is equal to the intensity of the same sample in the "off" state (pH = 10.5), only individual dendrimers are present. In the present case, this occurs for a loading ratio of $l \approx 0.5$.

For Ar27, sizes range between 16 nm < R_h < 35 nm for loading ratios 1.3 < l < 1.8. Distributions are of similar width (σ = 0.22 ± 0.08). Radii of gyration values span from R_g = 20 nm to R_g = 40 nm and R_g/R_h lies between 0.9 and 1.2, indicating less anisotropic structures than for Ar26. The dependency of the scattering intensity on loading ratio shows that interconnection of individual dendrimers starts at $l \approx 0.75$. Ar44 and Ar18 both form assemblies, but to a lower extent than Ar26 and Ar27; the threshold for the onset of dendrimer interconnection as determined from the scattering intensity is about $l \approx$ 1.0 for Ar44 and $l \approx 1.2$ for Ar18. Hydrodynamic radii for understoichiometric assemblies are lower, for l = 1.8 around R_h = 20 nm for both dyes, as visible in Figure 1a. Overall, light scattering of dendrimer−dye assemblies shows that the size depends on the loading ratio in an approximately linear relationship for about $l \leq 1.8$ and then increases more steeply toward l = 2, and size distributions are very narrow as compared to other ionically self-assembled systems.[29]

AFM was performed on Ar26/G4 assemblies with varying loading ratios. Samples were deposited on freshly cleaved mica surfaces. The oppositely charged surface may disintegrate the particles to a certain extent upon deposition and the solvent drain from hydrated structures can also influence the results. All findings therefore have to be compared with other methods if conclusions about the solution structure are desired. If this is done, it is, however, of interest to compare results and to test whether assemblies can be deposited on surfaces without disintegration. Images given in Figure 2 show elongated particles for all l, which corresponds well with the SANS results reported before.[52,55] The fact that imaging is possible on a negatively charged mica surface indicates that the particles likely are positively charged. In addition, it is evident that the assembly size increases with loading ratio being consistent with the light scattering results.

Furthermore, it is interesting to observe which fraction of the dendrimer gets interconnected into larger assemblies, which is possible with AFM as individual dendrimers are known to adsorb to mica surfaces in a wide pH range.[83] At l = 1 (Figure 2a) there are very few larger particles but predominantly individual smaller structures on the surface, which may be individual dendrimers. This is consistent with the finding from light scattering that dendrimers hardly get interconnected at low loading ratios. With increasing l, more large particles are visible. That is, individual dendrimers more likely become interconnected due to the increase in dye load (Figure 2b, l = 1.5). This can be confirmed by scaling all images like Figure 2a to a height scale with 10 nm maximum height (not shown), as then it is visible that the number of individual dendrimers on

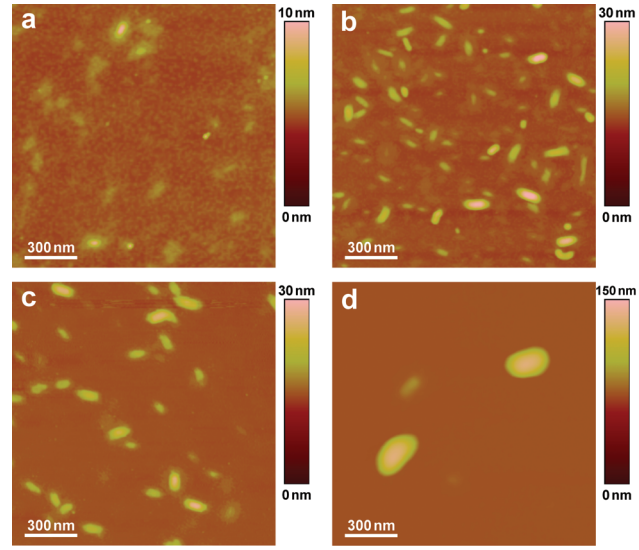

Figure 2. AFM for Ar26/G4 samples with different loading ratio deposited on mica: (a) l = 1.1; (b) l = 1.5; (c) l = 1.8; (d) l = 1.95.

the surface decreases with increasing l. When l approaches charge stoichiometry, the number of particles decreases again as the larger assemblies incorporate more individual dendrimers. This can be clearly observed in Figure 2d, where only large particles are present. These results support the conclusion from light scattering that for low loading ratios the majority of dendrimer molecules does not get interconnected, whereas the fraction of dendrimers comprising larger assemblies increases when approaching l = 2. Thus, if a high degree of dendrimer interconnection is desired, loading ratios 1.5 < l < 2 must be applied. That is since with increasing l the negatively charged dye molecules reduce the electrostatic repulsion between the cationic dendrimer molecules and mutual dye−dye interaction increases, both facilitating dendrimer aggregation.

AFM images can further be analyzed to obtain statistical size information. Results shown in Table 1 reveal an increasing average size of the particles with increasing loading ratio, whereas the aspect ratio decreases. The latter suggests that the potential of Ar26 to create anisotropic structures depends on the loading ratio. While care has to be taken when comparing AFM results to light scattering due to the possible changes in size and geometry through AFM sample preparation, the size range complies with the dimension from light scattering. Radii R^{calc} calculated for a volume-equivalent sphere from the particle volume estimated from AFM data allow for a semiquantitative comparison of sizes determined from both methods. It shows that radii are in the same order of magnitude but AFM radii are substantially smaller than hydrodynamic radii from light scattering. This is expected even for intact assemblies due to the shrinkage upon drying. The volume in the dried state is 27−45% of the volume corresponding to a sphere with the radius R_h from light scattering. This is reasonable as the hydrophilic assemblies are expected to be highly swollen in the solution. However, a further size reduction due to partial disintegration of the structures when deposited on the surface cannot be excluded. This is in particular suggested by the size distributions in AFM being broader than in light scattering ($\sigma \approx 0.3$ to 0.4 in AFM as compared to σ = 0.12 to 0.2 in light scattering), which may originate from such disintegration effects. In addition, there may be residual salt attached to the assemblies despite rinsing, broadening the distribution in AFM. Despite these details, overall it can be concluded that samples can be deposited and dried on mica surfaces without dramatic structural reorganization.

TABLE 1: Statistical Data from AFM Analysis

sample	l	length/nm	width/nm	height/nm	length/width	volume/1000 nm^3	R^{calc}/nm
Ar26/G4	1.03	94 (±30)	36 (±11)	4.2 (±0.8)	2.6	14	15
Ar26/G4	1.55	109 (±43)	40 (±18)	9.3 (±4.7)	2.7	41	21
Ar26/G4	1.79	138 (±54)	60 (±22)	17 (±10)	2.3	141	32
Ar26/G4	1.94	225 (±73)	115 (±52)	38 (±18)	2.0	983	61
Ar27/G4	1.79	–	175 (±48)	core: 6.4 (±2.2)	1.0	117	30

Ar27/G4 assemblies were also imaged by AFM. As seen in Figure 3, the particles clearly possess a core−shell type structure as was also found by SANS measurements.[55] Figure 3 also depicts a height profile. The low height suggests that the assemblies sprite on the surface in analogy to a "fried egg". Like for Ar26/G4 assemblies, the size corresponds approximately to light scattering. Some of the particles seem to have a larger core than others, which might originate from deformation on drying or residual salt.

Ar26 and Ar27 thus represent two different dye molecules, one being divalent and one trivalent and the former having an aromatic and hydrophobic moiety which is spatially separated from the hydrophilic part of the molecule, whereas the latter has a more symmetric charge distribution and no hydrophobic moiety. Due to the different ion valency and geometry, also the dimerization tendency substantially differs (see subsection E). We found this to lead to elongated structures for Ar26 and isotropic (core−shell) or flatlike (vesicle wall) structures for Ar27. Interestingly, it was found in a very different system based on a dye−surfactant combination that elongated structures were formed only if the hydrophobic moiety of the azo dye is spatially separated from the hydrophilic part of the molecule.[84] The structural difference in the dye molecules and thereby the different interplay of interactions thus represents a code for a particular assembly shape.

Finally, it should be mentioned that also Ar18/G4 and Ar44/G4 assemblies could be deposited and imaged on mica surfaces (see Supporting Information). The low height of the Ar18/G4 sample, however, may indicate a decreased assembly integrity upon deposition and drying as compared to Ar26/G4 and Ar27/G4, which is in accordance with the lower enthalpy of association reported previously.[55]

In conclusion, AFM confirmed light scattering and SANS results assemblies in terms of shape and size range. Additionally, an increase in size with loading ratio l was found both in AFM and light scattering. Scattering intensity and AFM pictures showed that between $l = 1$ and $l = 2$ the predominant species shifts from individual dendrimers to interconnected assemblies. Sizes and dendrimer interconnection abilities as determined from light scattering decrease in the order Ar26 > Ar27 > Ar44 ≈ Ar18, which is likely related to different thermodynamic parameters and further discussed in subsection E.

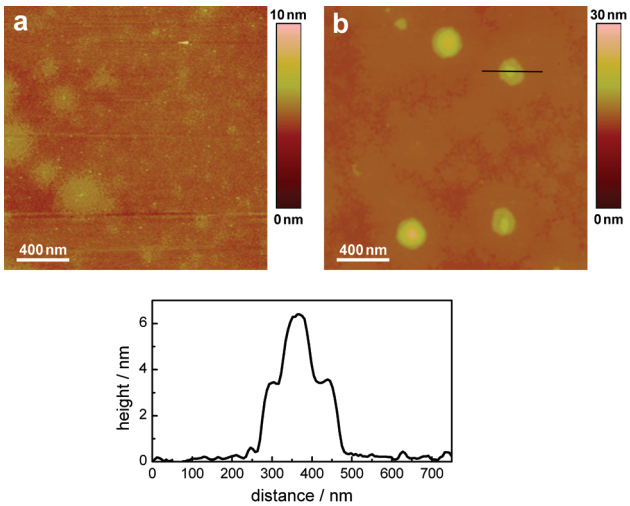

Figure 3. AFM of Ar27/G4 samples: (a) $l = 1.1$; (b) $l = 1.79$; (bottom) height profile corresponding to (b).

B. Stability Analysis by Zeta-Potential Measurements. For the Ar26 samples with dendrimer excess ($l < 2$), stability without precipitation is observed for several months for both investigated concentrations $c = 0.04$ g L^{-1} and $c = 0.005$ g L^{-1}. Results for the dyes Ar18, Ar27, and Ar44 are comparable. Previously, we postulated that the stability of the dendrimer−dye nanostructures in solution originates from their charge. This was demonstrated by ζ-potential measurements for other macroion−counterion systems.[51,57] ζ-potential is a good key to probe particle charge, as its value is proportional to the effective charge of a particle divided by its radius. The values of the ζ-potential for dendrimer−dye assemblies with Ar26 and Ar27 depicted in Figure 4 show that for $l \leq 2$ the ζ-potential is positive, corresponding to a positive net charge of the assemblies. This is reasonable, since there is an excess of positive charges from the dendrimer. The fact that the ζ-potential at charge stoichiometry is still positive is in accordance with earlier postulates of incomplete charge neutralization for example due to steric factors causing the assembly to be charge stabilized.[51−57] The dendrimer may also provide some additional steric stabilization. A similar dependency of ζ-potential on charge ratio was found for a polyelectrolyte−surfactant system showing that the excess component also determines the net charge in completely different systems.[85] The small decrease in ζ-potential in the range between $l = 1$ and $l = 2$ can be understood by the decrease of the average amount of charges left per dendrimer due to the increased dye load being partially compensated for by the increase in size and thus aggregation number. For samples with $l < 2$, the amount of free dye is negligible since there is an excess of dendrimer binding sites.

Figure 4 elucidates that slightly above charge stoichiometry the value of the ζ-potential crosses the value zero and the slope is highest. That is because approximately all dye molecules are

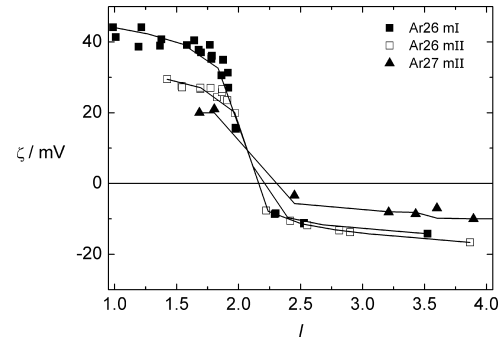

Figure 4. Zeta potential ζ in dependence on loading ratio l for Ar26/G4 and Ar27/G4 samples; c(G4) = 0.04 g L^{-1}; lines are to guide the eye.

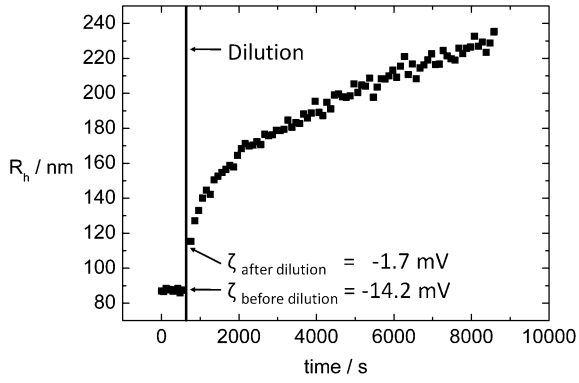

Figure 5. Zeta-potential and hydrodynamic radius of an Ar26/G4 sample with $l = 3$ before and after dilution.

associated with dendrimer at this loading ratio (c(G4) = 0.04 g L^{-1}) due to the high association constant. Therefore, the point of charge stoichiometry is also the point where aggregates are expected to be neutral. The fact that samples at and slightly above charge stoichiometry ($l = 2$) are stable for the lower concentration of $c = 0.005$ g L^{-1} for some of the dyes[52,55] can be understood by the fact that there is still a small amount of dye which is not attached to dendrimer molecules as the association constant has a finite value and there are geometric constraints for further aggregate growth. Once $2 < l < 2.2$ is passed, there is a change in ζ-potential to the negative. Between $l = 2$ and $l = 2.2$, measurements are not possible for the Ar26/G4 system, as the assemblies are too large and precipitation occurs quickly. The more l exceeds charge stoichiometry for those assemblies, the more negative the potential becomes. This means that excess dye can cause a charge reversal at $c = 0.04$ g L^{-1}. Another important finding is that the magnitude of the ζ-potential is larger for samples with $l < 2$, explaining the higher stability of the samples with excess of positively charged dendrimer, compared to excess of negatively charged dye. Samples with $l > 2$ at low dendrimer concentration ($c \approx 0.005$ g L^{-1}) were not stable for Ar26 and we found fast increases in hydrodynamic radius, which could be fitted very well with root functions.[52] In contrast, at the concentration used throughout this study ($c \approx 0.04$ g L^{-1}), assemblies with limited stability can be obtained for $l > 2.3$; that is, G4/Ar26 assemblies are stable in solution without size change for some days to few weeks before precipitation occurs. Radii are in the range between $R_h = 60$ nm at high l and $R_h = 300$ nm close to charge stoichiometry.

Concentration-dependent measurements, i.e., dilution experiments, can also serve to evaluate assembly stability, since changes in the absolute concentration can influence binding equilibria and therefore stability. Dilution of an Ar26/G4 sample with $l = 1.8$ by the factor of 8 (c(G4) ≈ 0.04 to ≈0.005 g L^{-1}) resulted in no major changes but only a slight increase in ζ-potential (ζ = 36 mV to ζ = 42 mV), which is expected due to a decrease in ionic strength. Assemblies do not change, likely because there is basically no dye dissociation (<0.01%) on dilution because of the high association constant and the excess of dendrimer binding sites, explaining the lack of concentration dependence for loading ratios $l < 2$. The ζ-potential also reveals a different concentration dependence for $l > 2$ as opposed to $l < 2$. Figure 5 depicts dynamic light scattering results together with ζ-potential findings for an Ar26/G4 sample with $l = 3$. It can be seen that the size of the sample at a dendrimer concentration of $c \approx 0.04$ g L^{-1} is constant at $R_h = 85$ nm and the ζ-potential is around ζ = −14 mV. Dilution by the factor eight to $c \approx 0.005$ g L^{-1} results in immediate growth of the colloidal particles and a strong increase in ζ-potential to ζ = −1.7 mV.

These findings can be understood by a second binding mode for $l > 2$. As discussed before, cooperative binding of dye ions to dendrimers takes place until approximately charge stoichiometry with very high association constants. As described above, there is no free dye in solution for understoichiometric samples and dye dissociation can be neglected due to the high equilibrium constant. Thus, the absolute concentration does not change the ζ-potential significantly for samples with $l < 2$. This situation is different for $l > 2$ because the dendrimer charges are saturated and thus there is free dye in solution as shown by UV−vis spectroscopy.[55] Therefore, the absolute concentration of free dye depends on the absolute concentration of the sample. At high sample concentration, there is a higher absolute concentration of free dye in solution than for low concentrations. The mechanism proposed is that free dye can additionally adsorb to fully neutralized assemblies causing a charge reversal and thereby stabilize the assemblies in solution, which is the only possible cause of the more negative ζ-potential at high concentration.[86] As opposed to this, a low absolute concentration of the sample means that there is much less free dye available in solution which could adsorb to the assembly. Consequently, charge stabilization is much weaker and assemblies start coagulating on dilution on a time scale of minutes. One can hence conclude that the adsorption process has a much lower equilibrium constant than the electrostatic binding of the dye to the dendrimer. Taking into account that there is no electrostatic attraction and ion pair formation, the adsorption must be driven by $\pi-\pi$ interaction or hydrophobic interactions in between the dye molecules and even overcome the repulsion between the like-charged dyes. It can thus be expected that the binding constant will be in the order of magnitude of dye dimerization described before.[55]

Further, it is worthwhile to compare the behavior of Ar27, as this dye lacks the ability to self-aggregate without polyelectrolyte due to the large number of negative charges and no dimerization could be detected by ITC and UV−vis spectroscopy.[55] For Ar27 the stability of samples with $l > 2$ is much lower than for Ar26, which is evident from the lower absolute values for the ζ-potential in Figure 4. For example, a sample with $l = 3$ grows by about 10% on a time scale of an hour for Ar27. Therefore, the second binding mode is restricted to a very low extent as the electrostatic repulsion to overcome is larger than for Ar26.

Finally, it is of interest to compare different preparation methods. The comparison of ζ-potential measurements for both methods I and II in Figure 4 shows that the larger assemblies prepared according to method I have larger values for the ζ-potential, indicating a higher net charge in the $l < 2$ range. This may be a size effect, as method I samples also show larger radii.

In summary, ζ-potential measurements show that both excess dendrimer and excess dye can stabilize assemblies, while an excess of dendrimer is able to stabilize the colloidal particles more efficiently than an excess of dye. This is an extension to our earlier study in which we only reported growth and precipitation for $l > 2$ at the lower concentration of $c = 0.005$ g L^{-1}.[52] The concentration dependence of the stability for dye excess is due to the ability of Ar26 to cause a charge reversal if the concentration of free dye is sufficiently high. The ability of Ar26 for this second overstoichiometric binding mode is based on its potential for self-aggregation, which could be shown

SCHEME 2: Loading Ratio Dependent Assembly Formation in a Cationic Dendrimer−Anionic Dye System[a]

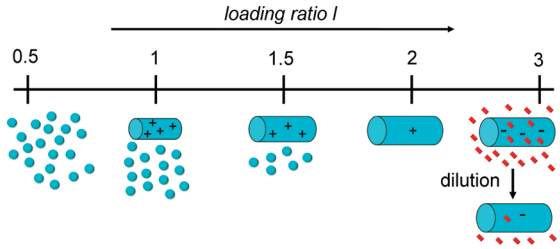

[a] Small spheres represent "individual dendrimers", cylinders larger assemblies, and red rectangles dye molecules. Bound dye molecules are not sketched for simplicity; "+" and "−" represent sign and relative magnitude of the assembly net charge.

by comparison to Ar27 that cannot self-aggregate and hence exhibits a lower degree of overbinding and thus lower assembly stability for $l > 2$. The behavior for Ar26 is summarized in Scheme 2.

C. Fraction of Large Assemblies and Assembly Composition by Centrifugation and Dialysis Experiments. The question which fraction of dendrimers becomes interconnected and why is important for establishing the approach in its versatility since large amounts of residual building blocks may not be desirable for certain applications. Light-scattering intensities and AFM pictures showed that the degree of interconnection of dye-loaded dendrimers increases with loading ratio. For the set of dyes under investigation, the loading ratio where no larger assemblies are present in solution was estimated as $0.5 < l < 1.2$. Because size distributions of the dendrimer−dye assemblies are very narrow, the amount of residual dendrimers can be determined by centrifugation without the risk of truncating the size distribution by sedimenting only a part of the particles. Supramolecular assemblies may change under gravitational force; hence, we chose our force applied as low as possible.[87] The amount of dye in the sediment and the supernatant is determined using UV−vis spectrometry before and after a centrifugation run. From UV−vis spectroscopy it is known that virtually all dye is bound to the dendrimer at a concentration of 0.05 g L^{-1} for $l < 2$, so the dye sedimenting must be incorporated into larger assemblies comprising multiple G4 molecules, whereas dye staying in solution is bound to dendrimers that are not part of larger assemblies. At the given setup (240 000g), it is possible to sediment assemblies with hydrodynamic radii above $R_h = 25$ nm even for small density differences. At charge ratios $l > 1.9$, all dye sediments, indicating full incorporation of the individual dendrimers into larger assemblies, which is consistent with AFM. The point where half of the dye molecules sediment is located at $l \approx 1.6$ (± 0.15). Lower loading ratios are close to the calculated lower size limit for which sedimentation is possible and thus we did not investigate loading ratios $l < 1.5$.

Centrifugation experiments also offer the possibility to probe the distribution of the dye molecules between larger assemblies and individual dendrimers, since the dye might not be uniformly distributed among all dendrimer molecules. To investigate this, an Ar26/G4 sample with $l = 1.79$ was centrifuged and the dried sediment dissolved in a sodium deuteroxide/deuterium oxide mixture. The supernatant was dried and dissolved likewise and both samples were investigated with NMR, as shown in Figure 6. (Spectra over the complete range of chemical shift from 1 ppm to 10 ppm are given in the Supporting Information.)

The ratio between one discrete signal of a specific methylene group at $\delta = 3.2$ ppm (all methylene group protons in α-position to the nitrogen of the amide group) in the dendrimer backbone was compared to the dye proton signals in the aromatic region. Specifically, the integral between $3.1 < \delta < 3.4$ ppm is normalized to $I = 248$, which is the number of protons in one perfect G4 PAMAM dendrimer molecule. The value of the integrals for the dye protons in the aromatic region thereby directly corresponds to the amount of dye molecules as all aromatic dye protons between a chemical shift of $\delta = 7.6$ and $\delta = 8.8$ give individual signals. Averaging the five aromatic proton integrals yields (53.7 ± 0.4) and (60.3 ± 0.3) dye molecules per dendrimer for the supernatant and the sediment respectively. This corresponds to a loading ratio of 1.68 for the

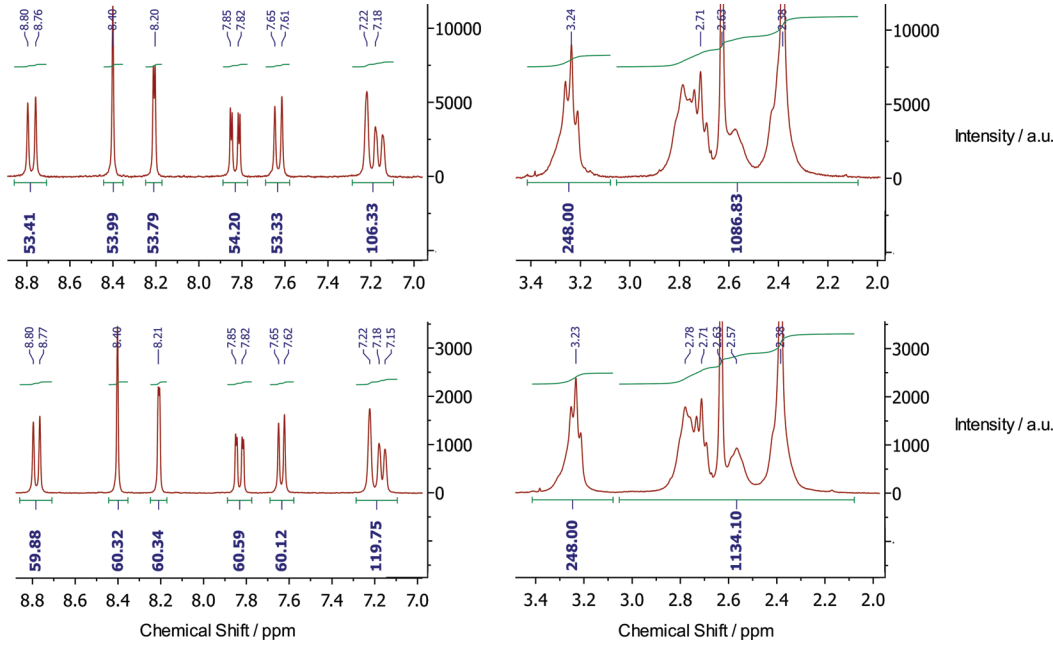

Figure 6. NMR spectra of the supernatant (top) and sediment (bottom) of a centrifugation experiment to analyze the composition of individual dye-loaded dendrimers and large assemblies: (left) aromatic region, only dye protons; (right) aliphatic region, dendrimer, and dye protons.

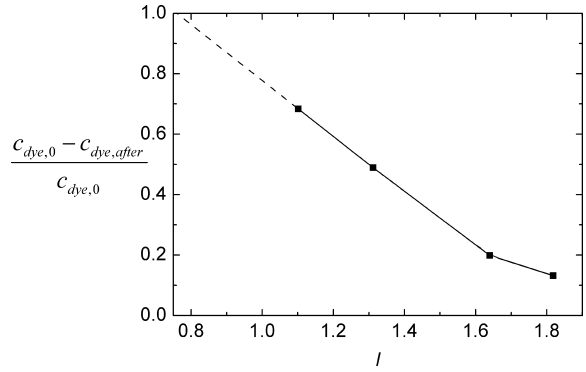

Figure 7. Dye release from a dialysis tube for Ar26/G4 assemblies as determined by UV−vis spectroscopy; c(G4) = 0.04 g L^{-1}; $c_{dye,0}$, initial dye concentration in the sample prior to dialysis, $c_{dye,after}$, dye concentration in the dialysis tube after dialysis; line to guide the eye.

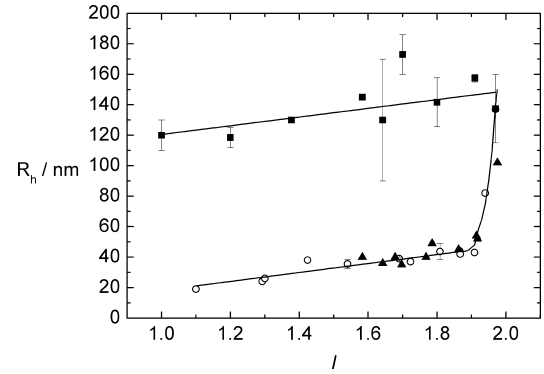

Figure 8. Hydrodynamic radius R_h versus loading ratio l for Ar26/G4 samples prepared via pH = 10.5 (open circles) and at pH = 3.5 (full squares) and at pH = 3.5 after pH change to pH = 10.5 and back to pH = 3.5 (closed triangles); c(G4) = 0.04 g L^{-1}.

supernatant, i.e., in the individual loaded dendrimers, and of 1.88 in the sediment, i.e., the larger aggregates. Hence, the dye in fact does not distribute homogeneously among the dendrimers but is enriched in the assemblies of interconnected dendrimers. The cooperative binding process of dye to dendrimer may cause such heterogeneous distribution. In large assemblies the number of dye−dye contacts is maximized, since the aromatic systems can interact more efficiently, which is energetically desirable.

Furthermore, dialysis experiments have been carried out with a set of Ar26/G4 samples. Whether dye is retained in the dialysis tube is due to the diffusion of individual dye-loaded dendrimers or small aggregates through the membrane, whereas dye incorporated in larger assemblies cannot pass through the membrane, which is guaranteed by the molecular weight cutoff of 100 kD. Even the smallest assemblies at $l = 1.1$ exceed this value by an order of magnitude. UV−vis spectra were taken before and after 2 weeks of dialysis to calculate the amount of dye released from the dialysis membrane. Results are displayed in Figure 7. Light scattering confirmed that the assemblies did not change during this time. It is evident in Figure 7 that the fraction of dye retained in the dialysis tube increases with loading ratio as the fraction of large assemblies unable to pass the membrane increases. The onset of aggregation is at the point where no larger assemblies but only individual dendrimers are present in solution and thus all dye is released from the dialysis tube. As determined from Figure 7, the point where $c_{dye,after} = 0$ lies around $0.6 < l < 0.9$, i.e., at a value $l < 1$. The point where half of the dendrimer-bound dye molecules migrate outside the dialysis tube is located at $l \approx 1.3 \pm 0.15$.

Hence, dialysis confirms light scattering and AFM results about the onset of aggregation below $l = 1$ for Ar26/G4-assemblies. In addition, centrifugation experiments have shown that the dye is not homogeneously distributed between larger assemblies and individual dendrimers but is enriched in the larger structures, suggesting that in the latter energetically favorable contacts between aromatic molecules are achieved more easily.

D. Kinetic versus Thermodynamic Effects in Assembly Formation. In previous studies we observed qualitatively that assemblies slowly dissolve upon addition of excess dendrimer, for example when changing the loading ratio from $l = 1.8$ to $l = 0.5$. This shows that structures are not kinetically trapped, but the dyes redistribute at least partially to the newly added dendrimer; i.e., the system readjusts to a change in loading ratio. From this it was concluded that the structures are in equilibrium with the building blocks. As the mentioned experiment is qualitative, a more rigorous study of the mixing procedure is of interest to understand the process of assembly formation in more detail. Since this process may take place on a very fast time scale, it is desirable to separate the steps of mixing the building blocks from the assembly formation. In the previous preparation technique (method I) where both building blocks are mixed at pH = 3.5, both processes take place simultaneously since the amino groups of the dendrimer are protonated. Mixing both components at pH = 10.5 and subsequent adjustment to pH = 3.5 (method II) offers the advantage that mixing can occur prior to assembly formation, as the amino groups of the dendrimer are deprotonated. Thus, assembly formation does not occur and therefore both components are already ideally mixed when the assembly formation is then induced by adding HCl. Certainly, there is also a kinetic effect of mixing the sample with HCl, but high local concentrations of either of the building blocks are avoided. Figure 8 shows the hydrodynamic radii of Ar26/G4 assemblies prepared according to methods I and II. The preparation method I at pH = 3.5 results in larger structures and larger standard deviations in size when comparing multiple samples with the same l. Sizes range from $R_h = 80$ nm to $R_h = 140$ nm for pH = 3.5 preparation and from $R_h = 20$ nm to $R_h = 50$ nm in case of the preparation via pH = 10.5. Furthermore, distributions are much more narrow for method II ($\sigma = 0.22 \pm 0.08$) than for method I ($\sigma = 0.35 \pm 0.17$). After changing the latter from pH = 3.5 to pH = 10.5 and back, assemblies of a comparable size to method II are obtained as is also depicted in Figure 8. A possible explanation for the size difference is an inhomogeneous distribution of the dye molecules, e.g., due to a strong cooperative binding process maximizing aromatic contacts, which leads to large assemblies enriched with dye and individual dendrimers with a lower average dye load. Hence, the formation of the supramolecular nanostructures in this system depends on the way of preparation to some extent and assemblies of different sizes can be obtained by choice of preparation route. To be able to compare assemblies of G4 PAMAM dendrimers with different dyes quantitatively, the same preparation method has to be used for all samples. Due to more ideal mixing conditions and as concluded from smaller assembly sizes, method II is likely to be less influenced by kinetic effects than method I, while a clear separation between thermodynamic and kinetic control is, however, difficult in this case. The role of kinetic effects likely depends on the strength of the interactions and thus electrostatic self-assembly of macroions and counterions can lead to thermodynamically controlled equilibrium structures independent of preparation route in some systems,[51,58] while in other systems assembly formation depends on preparation route; i.e., a kinetic influence is present for at

least one of the routes, in particular for high valent and/or strongly $\pi-\pi$ interacting counterions.[54,57] In further systems, it depended on the counterion used whether the preparation route plays a role or not, i.e. whether equilibrium structures were formed or kinetically trapped aggregates could be stabilized, both having defined size and morphology.[56] Having herein established a system where the same combination of building blocks can lead to differently controlled assemblies may open a route to an even more complex structure design of supramolecular assemblies, in analogy to molecular chemistry taking advantage of different reaction products resulting from different preparation routes.

E. General Discussion of Dendrimer−Dye Assemblies. It is highly desirable to reveal a correlation of the characteristics of a certain assembly with the characteristics of the building blocks and with thermodynamic data, which is why in this paragraph results of this study are further put into the context of results from the previous study.[55] Centrifugation, dialysis, light scattering, and AFM as presented herein give strong evidence that the predominant species for samples with low loading ratios prepared through method II are individual dendrimers loaded with dye, whereas around charge stoichiometry this species is not present (Scheme 2). Therefore, in a simplified view, the interplay between electrostatic repulsion due to residual charge of the dendrimers and attractive $\pi-\pi$ interactions and macroion−counterion electrostatics is decisive whether larger assemblies can be formed or not. The counterplay of forces is also responsible for the resulting assembly size. At the same time, residual charge is what prevents the larger assemblies from coagulation. Hence, there is only a specific range of charge ratios where stable larger assemblies incorporating the majority of dendrimers can be obtained, that is, for loading ratios $1.5 \leq l \leq 2$. The strong dependence of the assembly formation on charge ratio is due to the high association equilibrium constant in the order of $K = 10^6-10^7$ L mol^{-1}.[55] Ar26 yields the largest assembly size, i.e., has the highest "interconnection ability", followed by Ar27, whereas Ar18 and Ar44 yield particles with the smallest sizes and have higher onset points for interdendrimer aggregation. Interestingly, the trend for the association enthalpy per dendrimer decreases in the same order: ΔH(Ar26/G4) = −3013 kJ mol^{-1}, ΔH(Ar27/G4) = −2419 kJ mol^{-1}, ΔH(Ar18/G4) = −2242 kJ mol^{-1}, ΔH(Ar44/G4) = −2269 kJ mol^{-1}.[55] Thus, this strongly suggests that a connection into larger assemblies is due to the higher magnitude of the exothermic interaction enthalpy, which in this system turned out to play the main role for the free energy gain.

As discussed previously, the formation of ion pairs together with $\pi-\pi$ interaction between dye molecules and geometric effects can lead to the formation of defined assemblies of interconnected macroions,[51−59] the latter including the geometric properties of the dendrimer that due to its special architecture and semiflexibility can adopt different conformations but is not completely flexible under external forces such as electrostatics, interfacial effects or supramolecular association.[88−90] Experiments reported herein further suggest that high dye−dye interaction energies are a possibility to increase assembly size. This is consistent with the loading ratio dependency of the size as higher loading ratios also lead to more mutual interaction of the dye molecules. For example, the enthalpy for dye−dye stacking is ΔH(Ar26) = −30 kJ mol^{-1} and ΔH(Ar44) = −21 kJ mol^{-1}.[55] Since the amount of ion pairs is approximately the same for all four dyes, the surplus of interaction energy in case of Ar26 compared to Ar18, Ar27, and Ar44 should be due to $\pi-\pi$ interactions, thus supporting the correlation of higher dye−dye interaction energy with larger assembly size. This is a quite interesting finding, also because the set of dyes includes di- and trivalent dyes. One might have expected larger assemblies for the trivalent rather than a divalent counterion (Ar26), but the opposite is the case. In this context, one may regard that dye stacking induced by the dendrimer molecules can also lead to "pseudomultivalency" of counterions; i.e., a stack of several dye molecules with strong attractive $\pi-\pi$ stacking energy may be regarded as a counterion having both multifold charges and a special geometry. UV−vis spectroscopy had revealed that all dyes exhibit their strongest spectral changes relative to the free dye for loading ratios close to $l = 2$.[55] If l is decreased further, i.e. (as shown herein) in the range where assemblies dissolve at low loading ratios, spectral changes are partially reversed, indicating a decrease in $\pi-\pi$ interaction and thus loss of stacking energy. This represents further evidence in addition to the thermodynamic data that dye−dye interaction is a decisive factor in the formation of large assemblies.

While thus a relation of hydrodynamic size and enthalpy is elucidating, a size comparison based on R_h of course does not explicitly consider the very different shapes of the various assemblies: most interestingly, Ar26 gives anisotropic rodlike structures, while Ar27 yielded spherical core−shell aggregates with G4. This indicates, to a first approximation, that a stronger stacking enthalpy also causes formation of anisotropic structures. This is in accordance with results with naphthalenedicarboxylic acid counterions.[51] However, the different architecture of the counterion in terms of positions of charges and aromatic molecule parts certainly plays an additional role in this quite complex interplay, and the rodlike assembly shape for Ar26/G4 may also be a consequence of a direction through the specific Ar26 molecule structure. Further, it is interesting to note that both Ar26 and Ar27 have structures with a larger spatial distance of the sulfonate groups than Ar18 and Ar44, which may be a factor leading to higher enthalpies and thus larger potential for assembly formation.

All these issues concern the first binding process which is partly electrostatically driven. For $l > 2$, a further binding equilibrium of dye ions to the assemblies occurs with a much lower association constant, which, as depicted in Scheme 2, causes the stability dependency on absolute concentration in that regime. As this binding process is due to mutual dye interaction only, it only plays a role for the dyes with the higher dye−dye interaction energies, i.e., in particular for Ar26.

Hence, structural control in the approach of electrostatic self-assembly as presented herein in some sense is in analogy to encoding supramolecular structures with building blocks such as amphiphilic or crystallizing copolymers where packing controlled by nonlinear geometry is one of the effective codes.[91] In calculations, also the interplay of more than one type of interaction forces differing in directionality and range was shown to be a key to defined supramolecular particles, even if this involved only one kind of building block.[92] The additional advantage of the method in focus of the present study is the facile tunability of the magnitude of these interplaying interaction forces and of the directing building block architecture through choice and combination of easily available components. Toward a quantitative predictability of supramolecular assembly size and shape, however, further experimental studies and model development will be crucial.

Conclusion

In conclusion, we demonstrated that electrostatically self-assembled nanoparticles can be deposited on surfaces more or

less as intact entities and imaged by AFM, which confirmed the result from scattering in terms of size and shape. The assembly size was found to depend on loading ratio in a linear way and the onset of interdendrimer aggregation to lie around $l = 1$. At low loading ratios, assemblies coexist with individual dye-loaded dendrimers, in which the dye/dendrimer ratio is lower than in the larger assemblies. Around charge stoichiometry, only assemblies are present. The size of the assemblies depends on the dye counterion. Counterions with larger association enthalpies form larger aggregates and leave less noninterconnected dendrimers. Furthermore, the residual charge was shown to be the source of stability for all assemblies: for $l < 2$ the excess of positive charges from dendrimers and for $l > 2$ the excess of negative charges from dye ions provide stability. For $l > 2$ the dye can bind overstoichiometrically and cause a charge reversal through a second binding process with a much lower equilibrium constant than the electrostatic process, very likely due to $\pi-\pi$ interaction, a process only occurring if the free dye concentration is sufficiently high. This quantitative insight into the self-assembly of macroions and multivalent aromatic counterions will be of importance in further establishing this approach as route to versatile and functional nanostructures, in particular, developing a library of compounds which can lead to specifically desired assemblies with a certain size and shape.

Acknowledgment. Financial support of Deutsche Forschungsgemeinschaft, Verband der Chemischen Industrie (VCI), and the Interdisciplinary Center for Molecular Materials (ICMM, University Erlangen-Nürnberg) is gratefully acknowledged.

Supporting Information Available: AFM of Ar18/G4 and Ar44/G4 samples as well as full NMR spectra. This material is available free of charge via the Internet at http://pubs.acs.org.

References and Notes

(1) Ringsdorf, H.; Schlarb, B.; Venzmer, J. *Angew. Chem., Int. Ed. Engl.* **1988**, *27*, 113–158.
(2) Ikkala, O.; Brinke, G. T. *Science* **2002**, *295*, 2407–2409.
(3) Meister, A.; Bastrop, M.; Koschoreck, S.; Garamus, V. M.; Sinemus, T.; Hempel, G.; Drescher, S.; Dobner, B.; Richtering, W.; Huber, K.; Blume, A. *Langmuir* **2007**, *23*, 7715–7723.
(4) Zang, L.; Che, Y.; Moore, J. S. *Acc. Chem. Res.* **2008**, *41*, 1596–1608.
(5) Discher, D. E.; Eisenberg, A. *Science* **2002**, *297*, 967–973.
(6) Whitesides, G. M.; Grzybowski, B. *Science* **2002**, *295*, 2418–2421.
(7) Antonietti, M.; Förster, S. *Adv. Mater.* **2003**, *15*, 1323–1333.
(8) Percec, V.; Dulcey, A. E.; Balagurusamy, V. S. K.; Miura, Y.; Smidrkal, J.; Peterca, M.; Nummelin, S.; Edlund, U.; Hudson, S. D.; Heiney, P. A.; Duan, H.; Magonov, S. N.; Vinogradov, S. A. *Nature* **2004**, *430*, 764–768.
(9) Zakrevskyy, Y.; Stumpe, J.; Faul, C. F. J. *Adv. Mater.* **2006**, *18*, 2133–2136.
(10) Palmans, A. R. A.; Meijer, E. W. *Angew. Chem., Int. Ed.* **2007**, *46*, 8948–8968.
(11) Kaiser, T. E.; Wang, H.; Stepanenko, V.; Würthner, F. *Angew. Chem., Int. Ed.* **2007**, *46*, 5541–5544.
(12) De Greef, T. F. A.; Meijer, E. W. *Nature* **2008**, *453*, 171–173.
(13) Lee, E.; Kim, J. K.; Lee, M. *Angew. Chem., Int. Ed.* **2008**, *47*, 6375–6378.
(14) Murphy, R. J.; Pristinski, D.; Migler, K.; Douglas, J. F.; Prabhu, V. M. *J. Chem. Phys.* **2010**, *132*, 194903/1−6.
(15) Lehn, J. M. *Angew. Chem., Int. Ed.* **1988**, *27*, 89–112.
(16) Sijbesma, R. P.; Beijer, F. H.; Brunsveld, L.; Folmer, B. J. B.; Hirschberg, J. H. K. K.; Lange, R. F. M.; Lowe, J. K. L.; Meijer, E. W. *Science* **1997**, *278*, 1601–1604.
(17) Schmuck, C.; Wienand, W. *Angew. Chem., Int. Ed.* **2001**, *40*, 4363–4369.
(18) Schlaad, H.; Krasia, T.; Antonietti, M. *J. Am. Chem. Soc.* **2004**, *126*, 11307–11310.
(19) Kelch, S.; Rehahn, M. *Macromolecules* **1997**, *20*, 6185–6193.
(20) Fontana, M.; Chanzy, H.; Caseri, W. R.; Smith, P.; Schenning, J.; Meijer, E. W.; Gröhn, F. *Chem. Mater.* **2002**, *14*, 1730–1735.
(21) Kurth, D. G.; Higuchib, M. *Soft Matter* **2006**, *2*, 915–927.
(22) Northrop, B. H.; Zheng, Y.-R.; Chi, K.-W.; Stang, P. J. *Acc. Chem. Res.* **2009**, *42*, 1554–1563.
(23) Wang, M.; Zheng, Y.-R.; Ghosh, K.; Stang, P. J. *J. Am. Chem. Soc.* **2010**, *132*, 6282–6283.
(24) Wang, H.; Wang, S.; Su, H.; Chen, K.-J.; Armijo, A. L.; Lin, W.-J.; Wang, Y.; Sun, J.; Kamei, K.; Czernin, J.; Radu, C. G.; Tseng, H.-R. *Angew. Chem., Int. Ed.* **2009**, *48*, 4344–4348.
(25) Förster, S.; Hermsdorf, N.; Leube, W.; Schnablegger, H.; Regenbrecht, M.; Akari, S. *J. Phys. Chem. B* **1999**, *103*, 6657–6668.
(26) Boekhoven, J.; van Rijn, P.; Brizard, A. M.; Cohen Stuart, M. A.; van Esch, J. H. *Chem. Commun.* **2010**, *46*, 3490–3492.
(27) Antonietti, M.; Conrad, J.; Thünemann, A. *Macromolecules* **1994**, *27*, 6007–6011.
(28) Guan, Y.; Antonietti, M.; Faul, C. J. *Langmuir* **2002**, *18*, 5939–5945.
(29) Thünemann, A. F.; Müller, M.; Dautzenberg, H.; Joanny, J.-F.; Löwen, H. *Adv. Polym. Sci.* **2004**, *166*, 113–171.
(30) Franke, D.; Vos, M.; Antonietti, M.; Sommerdijk, N. A. J. M.; Faul, C. F. J. *Chem. Mater.* **2006**, *18*, 1839–1847.
(31) Duschner, S.; Störkle, D.; Schmidt, M.; Maskos, M. *Macromolecules* **2008**, *41*, 9067.
(32) Moreno-Villoslada, I.; Soto, M.; Gonzalez, F.; Montero-Silva, F.; Hess, S.; Takemura, I.; Oyaizu, K.; Nishide, H. *J. Phys. Chem. B* **2008**, *112*, 5350–5354.
(33) Schacher, F.; Betthausen, E.; Walther, A.; Schmalz, A. H.; Pergushov, D. V.; Müller, A. H. E. *ACS Nano* **2009**, 2095.
(34) Lemmers, M.; Sprakel, J.; Voets, I. K.; van der Gucht, J.; Cohen Stuart, M. A. *Angew. Chem., Int. Ed.* **2010**, *49*, 708–711.
(35) Schmuck, C.; Rehm, T.; Klein, K.; Gröhn, F. *Angew. Chem., Int. Ed.* **2007**, *46*, 1693–1697.
(36) Börner, H. G.; Smarsly, B. M.; Hentschel, J.; Rank, A.; Schubert, R.; Geng, Y.; Discher, D. R.; Hellweg, T.; Brandt, A. *Macromolecules* **2008**, *41*, 1430–1437.
(37) Frauenrath, H.; Jahnke, E. *Chem.—Eur. J.* **2008**, *10*, 2942–2955.
(38) Würthner, F. *Chem. Commun.* **2004**, 1564–1579.
(39) Hoeben, F. J. M.; Jonkheijm, P.; Meijer, E. W.; Schenning, A. P. H. J. *Chem. Rev.* **2005**, *105*, 1491–1546.
(40) Lohr, A.; Lysetska, M.; Würthner, F. *Angew. Chem., Int. Ed.* **2005**, *44*, 5071–5074.
(41) Percec, V.; Glodde, M.; Peterca, M.; Rapp, A.; Schnell, I.; Spiess, H. W.; Bera, T. K.; Miura, Y.; Balagurusamy, V. S. K.; Aqad, E.; Heiney, P. A. *J. Am. Chem. Soc.* **2007**, *129*, 11265–11278.
(42) Ryu, J.-H.; Hong, D.-J.; Lee, M. *Chem. Commun.* **2008**, 1043–1054.
(43) Bhosale, S. V.; Janiab, C. H.; Langford, S. J. *Chem. Soc. Rev.* **2008**, *37*, 331–342.
(44) Moreno-Villoslada, I.; Torres, C.; Gonzalez, F.; Soto, M.; Nishide, H. *J. Phys. Chem. B* **2008**, *112*, 11244–11249.
(45) Zhang, X.; Rehm, S.; Safont-Sempere, M. M.; Würthner, F. *Nature Chem.* **2009**, *1*, 623–629.
(46) Chen, Z.; Lohr, A.; Saha-Moller, C. R.; Würthner, F. *Chem. Soc. Rev.* **2009**, *38*, 564–584.
(47) Moreno-Villoslada, I.; Torres, C.; Gonzalez, F.; Shibue, T.; Nishide, H. *Macromol. Chem. Phys.* **2009**, *210*, 1167–1175.
(48) Gonzalez-Rodrıguez, D.; Janssen, P. G. A.; Martin-Rapun, R.; de Cat, I.; de Feyter, S.; Schenning, A. P. H. J.; Meijer, E. W. *J. Am. Chem. Soc.* **2010**, *132*, 4710–4719.
(49) Moreno-Villoslada, I.; Torres-Gallegos, C.; Araya-Hermosilla, R.; Nishide, H. *J. Phys. Chem. B* **2010**, *114*, 4151–4158.
(50) Smulders, M. M. J.; Nieuwenhuizen, M. M. L.; de Greef, T. F. A.; van der Schoot, P.; Schenning, A. P. H. J.; Meijer, E. W. *Chem.—Eur. J.* **2010**, *16*, 362–367.
(51) Gröhn, F.; Klein, K.; Brand, S. *Chem.—Eur. J.* **2008**, *14*, 6866–6869.
(52) Willerich, I.; Gröhn, F. *Chem.—Eur. J.* **2008**, *14*, 9112–9116.
(53) Gröhn, F. *Macromol. Chem. Phys.* **2008**, *209*, 2295–2301.
(54) Ruthard, C.; Maskos, M.; Kolb, U.; Gröhn, F. *Macromolecules* **2009**, *42*, 830–840.
(55) Willerich, I.; Ritter, H.; Gröhn, F. *J. Phys. Chem. B* **2009**, *113*, 3339–3354.
(56) Li, Y.; Yildiz, U. H.; Müllen, K.; Gröhn, F. *Biomacromolecules* **2009**, *10*, 530–540.
(57) Yildiz, U. H.; Koynov, K.; Gröhn, F. *Macromol. Chem. Phys.* **2009**, *210*, 1678–1690.
(58) Reinhold, F.; Kolb, U.; Lieberwirth, I.; Gröhn, F. *Langmuir* **2009**, *25*, 1345–1351.
(59) Gröhn, F.; Klein, K.; Koynov, K. *Macrom. Rap. Comm.* **2010**, *31*, 75–80.
(60) Willerich, I.; Gröhn, F. *Angew. Chem. Int. Ed.* **2010**, *49*, 8104−8108.

(61) Gröhn, F. *Soft Matter* **2010**, *6*, 4296–4302.
(62) We herein use the expression "assembly" to indicate supramolecular objects that possess a certain size and surface, i.e., have a narrow size distribution and a defined shape and are stable in aqueous solution, as different from "aggregates" which we regard as a more general term that may refer to such assemblies but also includes aggregates with broad size distribution, fractal character, etc. Other expressions for the assemblies discussed herein may be "self-assembled nanoparticles" or "supramolecular nano-objects".
(63) Ober, C. K.; Wegner, G. *Adv. Mater.* **1997**, *9*, 17–31.
(64) Koltover, I.; Salditt, T.; Rädler, J. O.; Safinya, C. R. *Science* **1998**, *281*, 78–81.
(65) Thünemann, A. F.; Beyermann, J. *Macromolecules* **2000**, *33*, 6878–6885.
(66) Decher, G. *Science* **1997**, *277*, 1232.
(67) Ariga, K.; Lvov, Y.; Kunitake, T. *J. Am. Chem. Soc.* **1997**, *119*, 2224–2231.
(68) Bharadwaj, S.; Montazeri, R.; Haynie, D. T. *Langmuir* **2006**, *22*, 6093–6101.
(69) Podsiadlo, P.; Kaushik, A. K.; Arruda, E. M.; Waas, A. M.; Shim, B. S.; Xu, J.; Nandivada, H.; Pumplin, B. G.; Lahann, J.; Ramamoorthy, A.; Kotov, N. A. *Science* **2007**, *318*, 80.
(70) Shchukin, D. G.; Grigoriev, D. A.; Möhwald, H. *Soft Matter* **2010**, *6*, 720.
(71) Ikeda, Y.; Beer, M.; Schmidt, M.; Huber, K. *Macromolecules* **1998**, *31*, 728–733.
(72) Schweins, R.; Huber, K. *Eur. Phys. J. E* **2001**, *5*, 117–126.
(73) Goerigk, G.; Huber, K.; Schweins, R. *J. Chem. Phys.* **2007**, *127*, 154908.
(74) Loh, P.; Deen, G. R.; Vollmer, D.; Fischer, K.; Schmidt, M.; Kundagrami, M.; Muthukumar, M. *Macromolecules* **2008**, *41*, 9352.
(75) Xu, Y.; Borisov, O. V.; Ballauff, M.; Müller, A. H. E. *Langmuir* **2010**, *26*, 6919.
(76) Kleinen, J.; Klee, A.; Richtering, W. *Langmuir* **2010**, *26*, 11258.
(77) Glotzer, S. C.; Solomon, M. J. *Nat. Mater.* **2007**, *6*, 557–562.
(78) Chen, T.; Zhang, Z.; Glotzer, S. C. *J. Phys. Chem. C* **2007**, *111*, 4132–4137.
(79) Provencher, S. W. *Comput. Phys. Commun.* **1982**, *27*, 229–242.
(80) DLS results in addition show a small peak (intensity 1−3%) at lower relaxation times which might be due to individual dendrimers or internal dynamic modes of the aggregate.
(81) The term "individual dendrimers" is used herein to name individual dendrimers as well as possibly aggregates of very few dendrimers, which are difficult observe by light scattering due to the small size and thereby small scattering intensity.
(82) For loading ratios in the diverging regime near $l = 2$, scattering intensities and hydrodynamic radii for some samples are effected by multiscattering of opalescent solutions and thus are included in the figure only partly.
(83) Pericet-Camara, R.; Papastavrou, G.; Borkovec, M. *Langmuir* **2004**, *20*, 3264–3270.
(84) Murakami, K. *Langmuir* **2004**, *20*, 8183–8191.
(85) Nizri, G.; Makarsky, A.; Magdassi, S.; Talmon, Y. *Langmuir* **2009**, *25*, 1980–1985.
(86) The value after dilution was measured immediately so that sizes before and after dilution are approximately the same eliminating the influence of particle size on ζ-potential.
(87) Tarabukina, E. B.; Krasnov, I. L.; Tarasova, E. V.; Ratnikova, O. V.; Melenevskaya, E. Yu.; Filippov, A. P.; Laukkanen, A.; Aseyev, V. O.; Tenhu, H. *Polym. Sci., Ser. A* **2008**, *50*, 198–205.
(88) Gröhn, F.; Bauer, B. J.; Amis, E. J. *Macromolecules* **2001**, *34*, 6701.
(89) Blaak, R.; Lehmann, S.; Likos, C. N. *Macromolecules* **2008**, *41*, 4452–4458.
(90) Lenz, D. A.; Blaak, R.; Likos, C. N. *Soft Matter* **2009**, *5*, 4542–4548.
(91) Palmer, L. C.; Velichko, Y. S.; Olvera de la Cruz, M.; Stupp, S. I. *Philos. Trans. R. Soc. A* **2007**, *365*, 1417–1433.
(92) Workum, K. V.; Douglas, J. F. *Phys. Rev. E* **2006**, *73*, 031502.

JP107358Q